Effect of Antimony and Cerium on the Formation of Chunky Graphite during Solidification of Heavy-Section Castings of Near-Eutectic Spheroidal Graphite Irons

P. LARRAÑAGA, I. ASENJO, J. SERTUCHA, R. SUAREZ, I. FERRER, and J. LACAZE

Thermal analysis is applied to the study of the formation of chunky graphite (CHG) in heavy-section castings of spheroidal graphite cast irons. To that aim, near-eutectic melts prepared in one single cast house were poured into molds containing up to four large cubic blocks 30 cm in size. Four melts have been prepared and cast that had a cerium content varying in relation with the spheroidizing alloy used. Postinoculation or addition of antimony was achieved by fixing appropriate amounts of materials in the gating system of each block. Cooling curves recorded in the center of the blocks show that solidification proceeds in three steps: a short primary deposition of graphite followed by an initial and then a bulk eutectic reaction. Formation of CHG could be unambiguously associated with increased recalescence during the bulk eutectic reaction. While antimony strongly decreases the amount of CHG, it appears that the ratio of the contents in antimony and cerium should be higher than 0.8 in order to avoid this graphite degeneracy.

DOI: 10.1007/s11661-008-9731-y

I. INTRODUCTION

HEAVY-SECTION castings made of spheroidal graphite are prone to graphite degeneration that leads to a dramatic decrease of the mechanical properties of the cast parts. Among the various forms of graphite degeneracy, chunky graphite (CHG) is certainly the most prominent. In usual cast irons, CHG forms in the central area (thermal center) of large castings, though it may appear also in thin sections.[1] Macroscopic observation shows a sharp transition, as illustrated in Figure 1, that could not be related to any significant macrosegregation.[2–4] Figure 2 illustrates the microstructure as most generally observed by optical microscopy in the areas affected by CHG. Noted first is the dendritelike ex-austenite with large nodules embedded in it, these latter being called primary nodules in the following discussion, and, second, cells of CHG and areas of usual eutectic SG microstructure with smaller nodules, which will be denoted as secondary nodules.

Solidification of heavy section castings is characterized by very slow cooling rates and lengthy eutectic plateau.[5–10] As the cast iron remains liquid for long periods of time, the melt may be affected by magnesium and inoculation fading, and this has been suggested as a possible reason for graphite degeneracy.[11] Accordingly, the use of chills has been found efficient to suppress CHG formation,[6,7,12,13] but this is limited to thicknesses up to a few centimeters. Graphite degeneracy in large section castings has often been related to the presence of low-level elements,[4,8,11,14–18] and limited additions of rare earths, lead, and antimony to the melt have been reported to help avoiding CHG formation.[11,17–20] However, these latter elements are pearlite promoter, and their addition should be strictly limited and controlled when a fully ferritic matrix is desired. Following these works, it appears that a clear understanding of CHG appearance and a safe mastering of metal preparation to avoid it are not yet available. In the present work, the solidification behavior of large blocks with or without addition of Sb and different levels of cerium are compared by means of the temperature/time records during casting and by means of microstructure observation. The results are discussed in view of previous similar reports, and both similarities and discrepancies are enlightened.

II. EXPERIMENTAL DETAILS

Cubic blocks with a size L of 300 mm were cast in sand molds according to the methodology described previously.[21] Their thermal modulus, *i.e.*, the ratio of their volume to their outer area for heat exchange with the mold, was about 5 cm. Each casting consisted of two to four blocks connected to the same gating system. Postinoculation and addition of Sb were performed as required by fixing appropriate materials with a foundry adhesive close to the selected block's entrance within the

P. LARRAÑAGA, I. ASENJO, and J. SERTUCHA, Research Engineers, and R. SUAREZ, Head, are with the Engineering and Foundry Department, AZTERLAN, E-48200 Durango (Bizkaia), Spain. I. FERRER, Engineer, is with TS Fundiciones, S.A. Pol. Sansinenea Erreka, E-20749 Arroa-Zestoa (Gipuzkoa), Spain. J. LACAZE, Senior Scientist, is with Université de Toulouse, CIRIMAT, UMR 5085, ENSIACET, 31077 Toulouse cedex 4, France. Contact e-mail: Jacques.lacaze@ensiacet.fr

Fig. 1—Central section of a cubic block (30 cm in size) with the zone affected by CHG appearing with darker contrast.

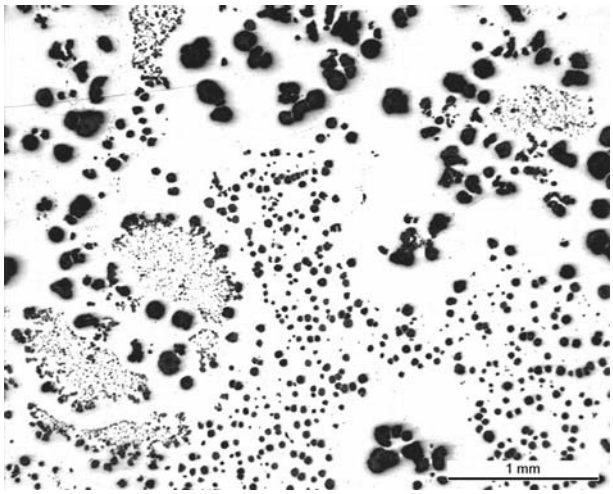

Fig. 2—Optical micrograph of a heavy-section SG cast iron block showing dendritelike ex-austenite with large nodules embedded in it, cells of CHG, and areas of usual SG microstructure.

gating system. Postinoculation was made with a commercial inoculant (70 to 78 Si, 3.2 to 4.5 Al, 0.3 to 1.5 Ca, and ~0.5 RE, in wt pct), while addition of Sb was performed with 99.99 pct pure element, to reach a level of 0.004 to 0.010 pct of the weight of the block. In the following, the various blocks will be labeled as M5-X-Y, where M5 is for the modulus of the blocks, X indicates the trial number (12, 13, 16, or 18 in the present report), and Y stands for blocks with either no postinoculation (N) or postinoculation (I), or else with postinoculation and addition of Sb (ISb). In the case of the M5-16 trial, two levels of Sb were added, which are differentiated with an additional label, a or b.

These four castings were made within a limited time in one single cast house so that it is expected that the charge materials were very similar. Table I gives the details of the trails and lists the composition of the four melts that were cast as measured on medals taken before pouring in the mold; the Sb content was obtained directly from the blocks using the ICP-MS technique. All other elements than those listed were at very low and reproducible levels.[21] The differences in the cerium content between trials that are observed in Table I are due to the use of various FeSiMg alloys for performing the nodularizing treatment. Besides, 0.034 pct of Ce-bearing misch metal was added to the melt during the nodularizing treatment performed during the M5-13 trial. The stable eutectic temperature of these alloys is predicted to vary from 1162.7 °C to 1163.3 °C depending on the composition.[22] The carbon equivalent, C_{eq}, reported in the table was calculated without accounting for the silicon added by the inoculation treatment and could be increased by about 0.04 because of it.

Most of the cast blocks were equipped with a single K-type thermocouple positioned at the geometrical center for recording the cooling curves during solidification and cooling. An additional thermocouple was located at L/6 from the outer surface of the two blocks cast during trial 18 (Figure 3). Because of a different conditioning of the blocks in this latter trial, the effective thermal modulus was higher than for the other castings at about 6 cm. Also, for all trials, and just before casting the blocks, some metal was poured in two standard TA cups, one of them containing powder of inoculant so as to reach the same level as for the blocks.

Table I. Code of Casting Trials; Indication of the Use of Postinoculation (I for Yes) or Not (N for No) and Addition of Sb (Sb); Composition of the Melt in Carbon, Silicon, Cerium, and Antimony (Weight Percent); Carbon Equivalent (Calculated as $C_{eq} = w_C + 0.28\ w_{Si}$[22]), and Microstructure Characteristics (Text)

Trial	Block	w_C	w_{Si}	w_{Ce}	w_{Sb}	C_{eq}	V_V	A_A	N_{block}	A_{PG}	N_{PG}	A_{SG}	N_{SG}
M5-12	ISb	3.68	2.20	0.0123	0.0095	4.30	0.5	1.0	90	44	15	55	150
	I				<0.0002		18.0	47.0	83	32	48	21	137
M5-13	N	3.73	2.08	0.0162	<0.0002	4.31	0.1	50.0	25	19	9	31	35
	I				<0.0002		15.0	14.0	63	32	41	54	76
	ISb				0.0108		2.0	7.0	94	25	64	68	105
M5-16	ISb-a	3.72	2.08	0.0100	0.0043	4.30	7.0	10.0	81	20	67	70	85
	ISb-b				0.0071		4.0	20.0	89	31	84	49	92
	I				<0.0002		22.0	5.0	110	21	110	74	110
	N				<0.0002		0.5	50.0	39	16	33	34	42
M5-18	ISb	3.71	2.07	0.0028	0.0095	4.29	0.0	0.0	70	16	49	84	74
	I				<0.0002		24.0	6.0	88	24	9	70	115

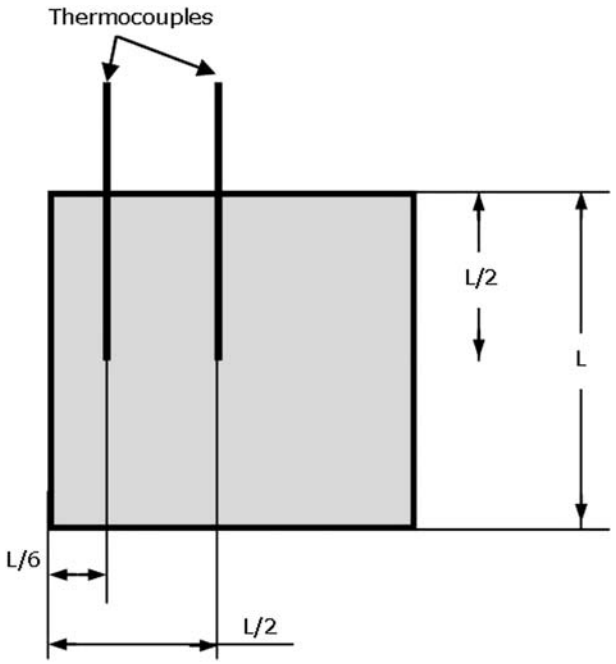

Fig. 3—Location of the K-type thermocouples in the blocks of the trial M5-18.

After casting, the blocks were sectioned and the volume fraction V_V affected by CHG was measured from images such as the one in Figure 1 where the zone affected by CHG was generally easily located because of the darker contrast. In order to evaluate V_V, two perpendicular central sections of each block were prepared, one with the entire section and the other with half of it.[21] Denoting S_1 the area affected by CHG in the first section, and $S_2/2$, the one in the half perpendicular section, an evaluation of the volume V of the CHG zone was made by means of the expression

$$V = \frac{2}{3\cdot\sqrt{\pi}}\cdot\left(S_1\sqrt{S_2} + S_2\sqrt{S_1}\right) \qquad [1]$$

which assumes an ellipsoid shape. This value was then normalized with the volume of the related block to give the fraction of the volume V_V affected by CHG.

Metallographic sections were then prepared from samples taken at the center of the casting, on which series of micrographs such as the one in Figure 2 were made for measuring the local area fraction A_A of CHG.[21] On similar sets of micrographs, the areas A_{PG} and A_{SG} with, respectively, primary and secondary graphite nodules, as well as the corresponding nodule densities N_{PG} and N_{SG} were estimated. The average nodule count N_{block} measured on the areas free of CHG (*i.e.*, on a fraction 100-A_A of the entire area) is given as the surface-weighted average counts of primary and secondary nodules:

$$(100\text{-}A_A) \times N_{block} = A_{PG} \times N_{PG} + A_{SG} \times N_{SG} \qquad [2]$$

All these values are also listed in Table I.

III. RESULTS

Cooling curves recorded by thermal analysis with standard TA cups are shown in Figures 4(a) and (b) for noninoculated and inoculated alloys, respectively. Both sets of curves show that solidification proceeds in two steps, much like the description given by Chaudhari *et al.*[23] for nearly eutectic alloys with an initial eutectic reaction and a more lengthy eutectic plateau. These curves confirm also that all four melts have similar solidification features as expected from their nearly identical C_{eq} (Table I). The effect of postinoculation appears to significantly increase the eutectic plateau temperature, except for trial M5-12, where this increase is limited. On the contrary, it is worth stressing that postinoculation left unchanged the temperature for the initiation of the solidification for these heat exchange conditions.

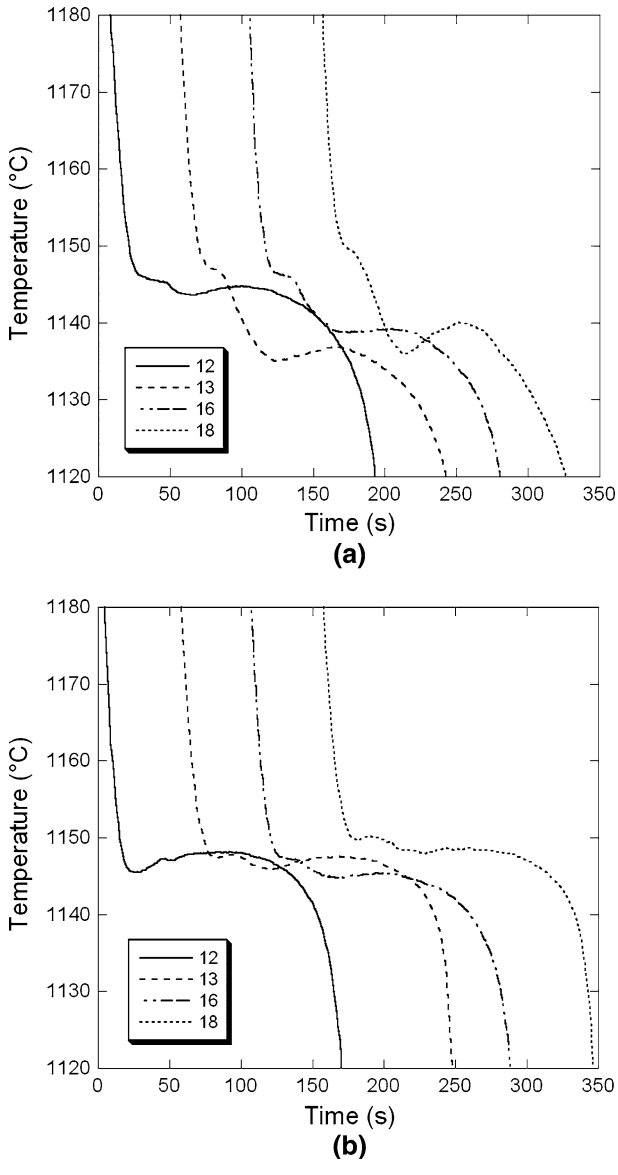

Fig. 4—Cooling curves recorded on the TA cups for melts (*a*) without and (*b*) with postinoculation.

None of the TA cups showed any CHG, so the cooling curves recorded on the blocks were first analyzed with the aim of looking for any difference with the TA cup records and for any relationship between their characteristics and the amount of CHG, as measured either with A_A or V_V. Figure 5(a) compares the cooling curves of blocks M5-13-N and M5-16-N without postinoculation, and Figure 5(b) is a representative micrograph of the central area of either block. While CHG is concentrated at the center of these blocks (very low V_V values, Table I and the figure), its local amount is quite large (high values of A_A). It is seen that the cooling curves present exactly the same features as those recorded on the TA cups with two marked eutectic reactions. However, an initial and very short thermal arrest that was not observed on the curves in Figure 4 appears in both curves in Figure 5(a). The shape of this arrest leads to its relation to nucleation of primary graphite, as discussed in Section IV.

However, it is puzzling that the initial eutectic temperature and then the bulk eutectic temperature of these two castings differ so much, where their microstructures appear so similar in terms of A_A and V_V values. The only difference that could be noted is in the value of N_{PG}, estimated at 33 and 9 mm^{-2} for blocks M5-16-N and M5-13-N, respectively. This will be discussed further later in this article. In Figure 5(a), it is also noteworthy than none of the eutectic arrests shows any significant recalescence, as could be expected from the high A_A associated values because the growth rate of CHG cells is expected to be much higher than the one of SG eutectic cells.[10] In other words, the characteristics of the cooling curves do not seem to relate to local microstructure evolution.

Figure 6(a) provides a comparison of the cooling curves recorded on postinoculated blocks without Sb added. In the case of M5-12-I block, the thermocouple broke before solidification completion. In all cases, the

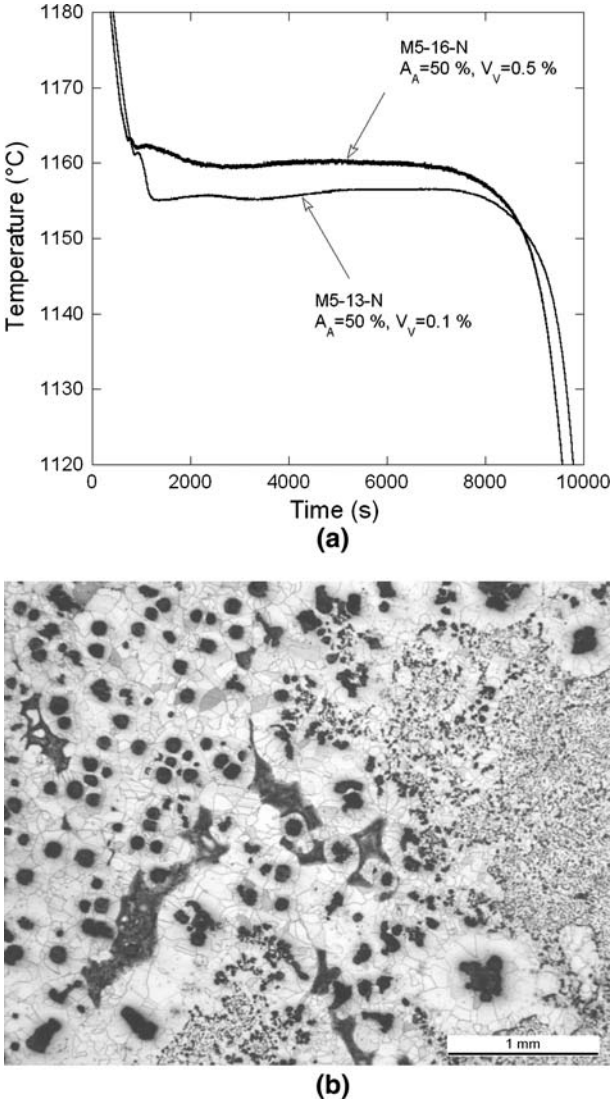

Fig. 5—(*a*) Cooling curves recorded on blocks M5-13-N and M5-16-N without postinoculation and (*b*) representative micrograph after etching with Nital.

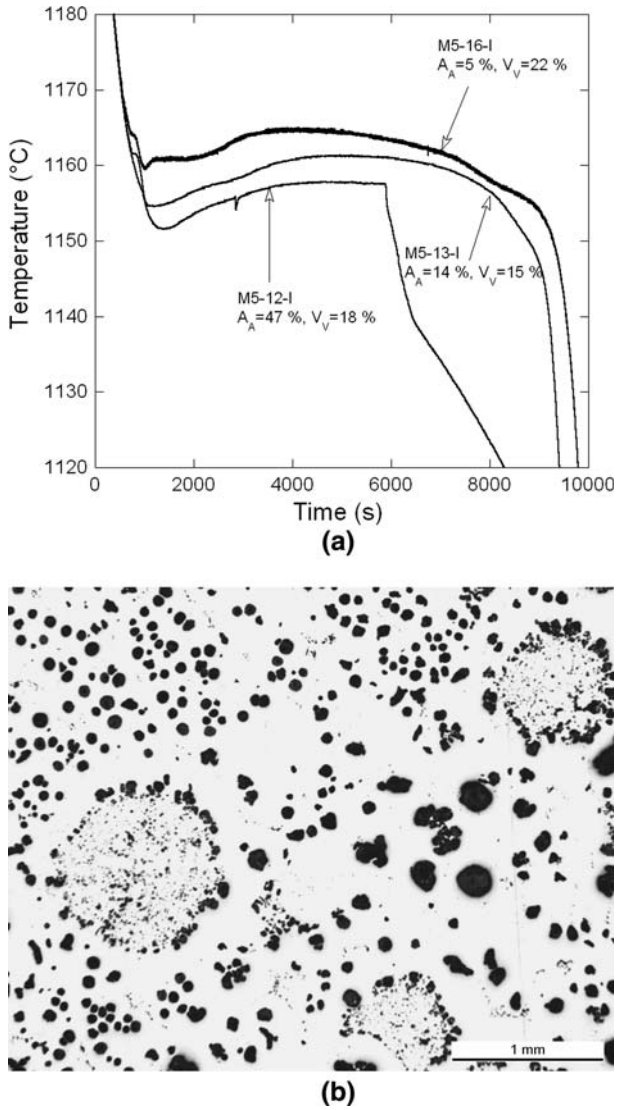

Fig. 6—(*a*) Cooling curves recorded on blocks M5-12-I, M5-13-I, and M5-16-I with postinoculation and (*b*) representative micrograph.

eutectic solidification proceeds again in two steps after a pre-eutectic reaction that is apparent for two of the three curves. The effect of inoculation is clearly evidenced when comparing Figures 5(a) and 6(a), with both eutectic reactions showing higher recalescence after postinoculation. As V_V increases also with postinoculation,[21] this higher recalescence could be related partly to the formation of CHG and partly to the increase in nodule count. As in Figure 5(a), the eutectic plateau temperatures are sorted according to the corresponding minimum temperatures, with the N_{PG} value much higher for block M5-16-I at 110 mm^{-2} than for the two others, 41 mm^{-2} and 48 mm^{-2} for blocks M5-13-I and M5-12-I, respectively. Figure 6(b) gives an example of the microstructure observed in these castings.

Finally, comparison of cooling curves for inoculated materials with Sb added is provided in Figure 7, where the record for the highest Sb addition has been selected for the M5-16 trial. The graph shows the same features as previously shown, though the two eutectic reactions have almost merged in one single thermal arrest for castings M5-12-ISb and M5-13-ISb. As previously found, the temperature for the start of the initial eutectic reaction decreases with N_{PG}, and the eutectic plateau temperatures are clearly sorted accordingly and do not appear to relate to A_A or V_V values.

These preliminary conclusions were confirmed by the analysis of the two cooling curves recorded on each of the blocks of trial M5-18. Figure 8(a) shows the cooling curves at L/6 and L/2 (thermal centre) of the block without Sb added. It is seen that the curves get nearly superimposed early during initial cooling and remain so for half of the solidification time of the entire block. The same observation could be made regarding the two cooling curves recorded on the block with Sb added. This means that, after an initial transient, the temperature of the material is homogeneous, the liquid cools, and then solidification begins in a nearly uniform way in the entire block. The cooling curves appear to be representative of the solidification at the scale of the blocks, thus explaining that no correlation between A_A and V_V and the eutectic plateau temperature can be observed.

A comparison of the records at the distance $L/6$ from the surface of the blocks with and without Sb added is made in Figure 8(b). The two curves are superimposed until about one-third of the solidification time, and then a strong recalescence appears in the case of the untreated block. Because the microstructure of these castings differs by the fact that Sb totally suppresses CHG while V_V is found to be equal to 24 pct in the nontreated block (Table I), it seems logical to associate the increase of the recalescence rate to the growth of CHG. Comparison of the curves at the center of the blocks showed exactly the same features, at exactly the same time, though the increase of the recalescence rate was slightly lower. This leads to the consideration that

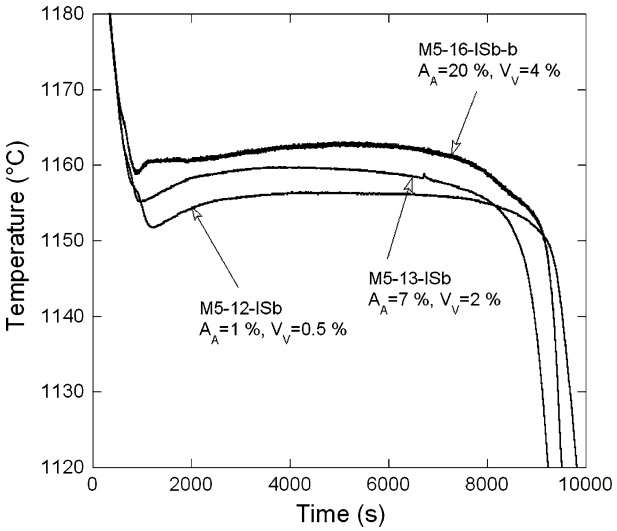

Fig. 7—Cooling curves recorded on blocks M5-12-ISb, M5-13-ISb, and M5-16-ISb-b with postinoculation and addition of Sb.

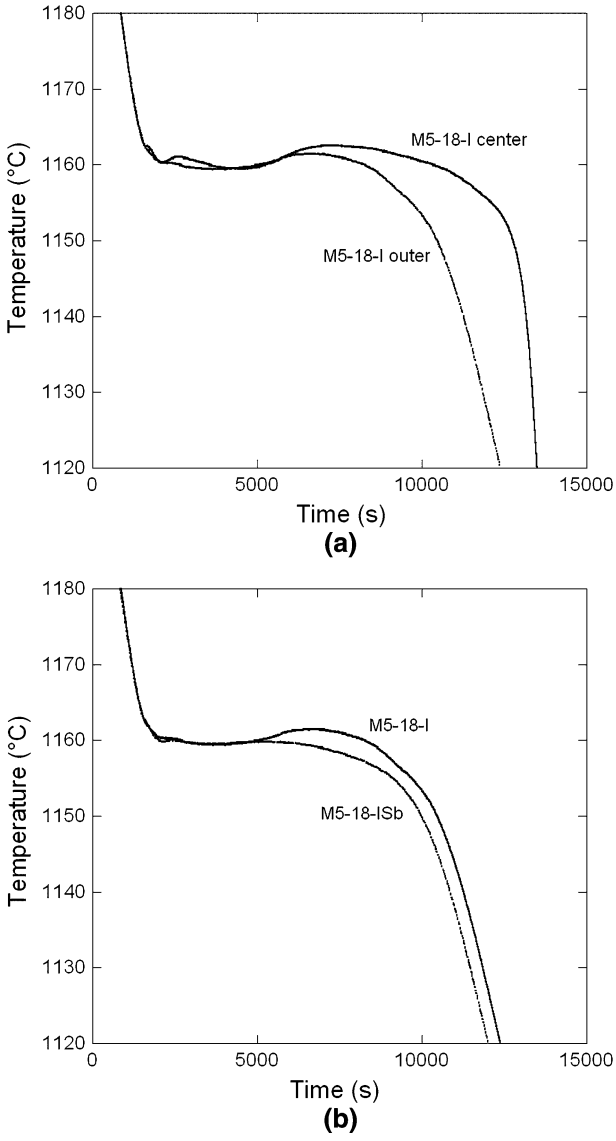

Fig. 8—Cooling curves recorded during the trial M5-18: (*a*) comparison for the center and outer locations of the inoculated blocks and (*b*) effect of Sb addition on the outer records.

successive solidification steps, nucleation of primary nodules and initial eutectic reaction, nucleation of secondary nodules as well as nucleation of the CHG cells, and bulk eutectic reaction proceed at about the same time in a major part of the blocks.

IV. DISCUSSION

From the results in Section III, it may be inferred that the initial eutectic reaction relates to the coupled growth of austenite and primary graphite nodules. This is in line with the schematic proposed for the formation of CHG by Zhou *et al.*[24] on the basis of experiments, where CHG cells appeared to form after significant development of austenite dendrites and primary nodules. It has been suggested previously that the first thermal arrest relates to primary graphite deposition, and this can be substantiated by considering the size of the nodules. For a growth proceeding by solid-state diffusion through the austenite shell, Wetterfall *et al.*[25] showed that the radius of the graphite nodules R may be written as

$$R^2 - R_0^2 \approx \alpha \cdot (t - t_0) \qquad [3]$$

with R_0 and t_0 being the initial size and time for nucleation and α being a temperature-dependant coefficient. Considering the nearly isothermal eutectic plateaus in Figure 5(a) and setting R_0 to zero, the ratio of the radii of the primary to the secondary nodules should then be of the order of $(7000/5000)^{0.5}$, *i.e.*, about 1.2. The fact that this ratio is experimentally much larger, as seen in the micrographs (Figures 2, 5(b), and 6(b)), shows that primary nodules have indeed grown for some time in direct contact with the liquid. This sustains the assumption that the short thermal arrest observed on the cooling curves of the blocks relates to precipitation of primary graphite nodules.

It was noted that postinoculation did not change the temperature of the first eutectic reaction, as observed with TA cups. Similarly, both the temperature for the primary arrest and the temperature for the first eutectic reaction were nearly identical in all blocks recorded from one melt. This is illustrated in Figure 9, where the cooling curves recorded on the three M5-13 blocks are compared. This observation is quite astonishing as the values of N_{PG} may differ greatly for one given melt depending on inoculation and addition of Sb (Table I). Indeed, it was found that the undercooling between the primary arrest and the start of the eutectic reaction is correlated with the amount of cerium, being respectively 2 °C, 4 °C, 5 °C, and 7 °C for Ce levels of, respectively, 0.003, 0.01, 0.0123, and 0.0162 wt pct. Such an effect has long been known[7] and suggests that cerium both decreases the nucleation rate of primary graphite and diminishes the graphite growth rate. Cerium thus seems to delay the establishment of the coupled reaction between austenite and graphite that leads to the initial eutectic reaction. As expected, however, once this reaction has started, the associated recalescence rate increases with the nodule count, *i.e.*, with the effectiveness of inoculation.

As a matter of fact, an increase of the recalescence rate could be observed after the initial eutectic reaction during the solidification of all castings that were inoculated but without Sb addition, as illustrated in Figure 9. It was first associated with the start of the bulk eutectic reaction, *i.e.*, related to nucleation of secondary graphite nodules, but is certainly due also to CHG formation or enhanced by it, as suggested by the analysis of Figure 8. This observation is much in line with the conclusions of Prinz *et al.*,[3] who reported that recalescence is limited when CHG is concentrated in the center of the castings and maximum when the entire section is affected. The relation between V_V and recalescence during bulk eutectic reaction, as observed during the present work, is illustrated in Figure 10. It is

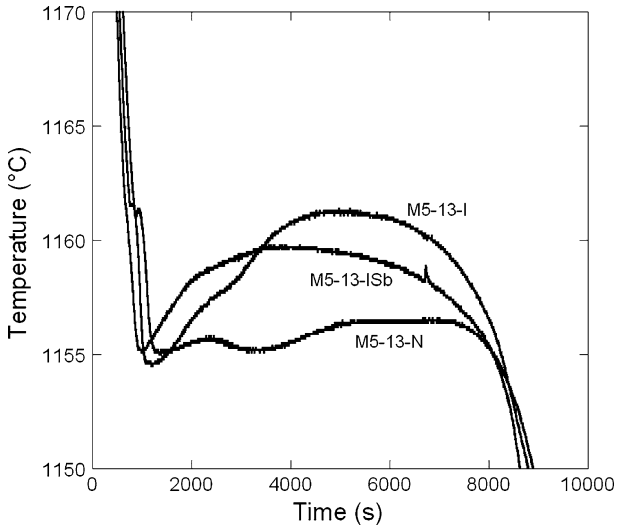

Fig. 9—Comparison of the cooling curves obtained at the thermal center of the three blocks of the trial M5-13.

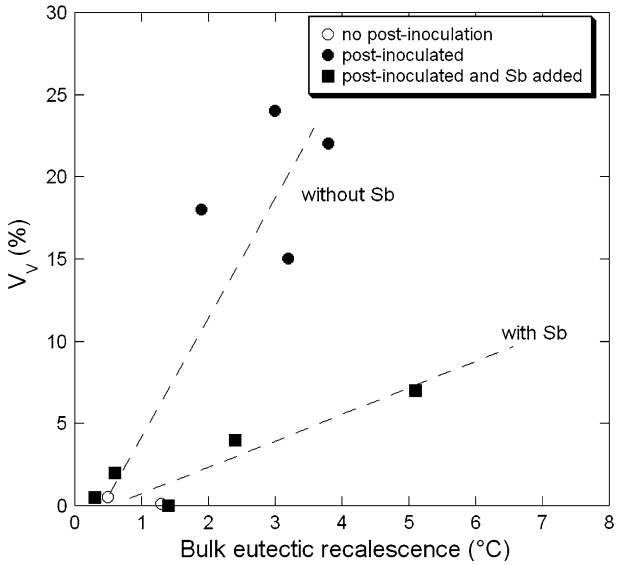

Fig. 10—Correlation between recalescence during the bulk eutectic reaction and V_V value.

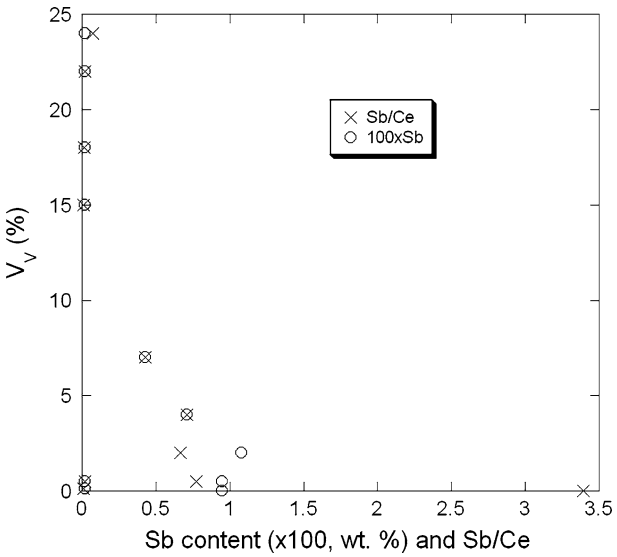

Fig. 11—V_V *vs* Sb content (100 times) and as function of the ratio of the Sb and Ce contents.

seen that the increase in V_V with recalescence is much less pronounced when Sb has been added. This may be tentatively related to a lower count in CHG cells after Sb addition, although no attempt has yet been made to evaluate it quantitatively.

The beneficial effect of Sb may be illustrated as well by plotting V_V as a function of Sb content, as done in Figure 11. Note that the points at the lower left corner (origin) of the graph relate to non-postinoculated melts that have been shown to be much less prone to CHG formation.[21] Although this effect of Sb addition in slow solidification conditions has been repeatedly reported in the literature, as reviewed by Javaid and Loper,[11] its efficiency may depend on the presence of other elements. As an example, Figure 11 also demonstrates the negative effect of Ce as a CHG promoter. When this element is present, higher additions of Sb are needed in order to prevent the formation of CHG, with a minimum Sb/Ce ratio of 0.8 for guaranteeing the avoidance of that defect, in agreement with previous results.[26] The interplay of cerium and antimony, the latter being known to increase the nucleation rate,[8,27] should be investigated further for a clearer understanding of the increased amount of CHG with nodule count, which was reported previously.[21]

V. CONCLUSIONS

It is concluded from the preceding results that solidification of the heavy section of near-eutectic spheroidal graphite cast irons starts with the precipitation of primary graphite nodules, followed by simultaneous growth of austenite with these nodules getting embedded in it. The CHG cells nucleate after this initial eutectic reaction has processed for some time, and their growth is made evident by an increased recalescence rate during the bulk eutectic reaction when compared with the case where no CHG forms. Owing to the very small composition differences between the alloys presently studied, it may be stated that the undercooling of the melt, *i.e.*, its supersaturation in carbon, greatly varied from one casting to another without a direct relation to the amount of CHG formed. This suggests that the proposal by Gagne and Argo,[2] that CHG increases with constitutional supercooling of the melt, should be further substantiated. One line for further work emerged by concordant observations that oxides or compounds found in CHG areas differ from those observed in unaffected zones.[4] As a matter of fact, the lengthy cooling and solidification time of heavy section SG irons may allow for significant changes in the amount of active elements dissolved in the melt. Accordingly, one may have to consider nucleation and growth of oxides or other compounds of Mg, Ce, or any other additive or impurity for a proper understanding of CHG formation.

ACKNOWLEDGMENTS

This article is based on work supported by the Industry Department of the Spanish Government (Grant No. PROFIT FIT-030000-2007-94). Thanks are due to Luiz Eleno for translating the German papers.

REFERENCES

1. R. Källbom, K. Hamberg, and L.E. Björkegren: *Proc. Gjutdesign 2005 Final Seminar*, VTT Technical Research Centre of Finland, Espoo, 2005, pp. 1–25.
2. M. Gagné and D. Argo: *Proc. Int. Conf. "Advanced Casting Technology,"* J. Easwaren, ed., ASM INTERNATIONAL, Metals Park, OH, 1987, pp. 231–56.
3. B. Prinz, K.J. Reifferscheid, T. Schulze, R. Döpp, and E. Schürmann: *Giessereiforschung*, 1991, vol. 43, p. 107.
4. R. Källbom, K. Hamberg, and L.E. Björkegren: *Proc. 67th World Foundry Congr.*, Harrogate, United Kingdom, 2006, paper no. 184.
5. C.R. Loper, R.W. Heine, R.W. Reesman, and B.H. Shah: *AFS Trans.*, 1967, vol. 75, pp. 541–47.
6. P.K. Basutkar and C.R. Loper: *AFS Trans.*, 1971, vol. 79, pp. 169–75.
7. P.K. Basutkar and C.R. Loper: *AFS Trans.*, 1971, vol. 79, pp. 176–85.
8. M. Wessén, I.L. Svensson, and R. Aagaard: *Int. J. Cast Met. Res.*, 2003, vol. 16, pp. 119–24.
9. Z. Ignaszak: *Int. J. Cast Met. Res.*, 2003, vol. 16, pp. 93–97.
10. R. Källbom, K. Hamberg, M. Wessén, and L.E. Björkegren: *Mater. Sci. Eng.*, 2005, vols. A413–A414, pp. 346–51.
11. A. Javaid and C.R. Loper, Jr.: *AFS Trans.*, 1995, vol. 103, pp. 135–50.
12. R.K. Buhr: *AFS Trans.*, 1968, vol. 76, pp. 497–503.
13. P.K. Basutkar, C.R. Loper, and C.L. Babu: *AFS Trans.*, 1970, vol. 78, pp. 429–34.
14. R. Barton: BCIRA Report, BCIRA, London, 1981, vol. 1436, pp. 340–53.
15. H. Itofuji and H. Uchikawa: *AFS Trans.*, 1990, vol. 98, pp. 429–48.
16. S.I. Karsay and E. Campomanes: *AFS Trans.*, 1970, vol. 78, pp. 85–92.
17. E.N. Pan, C.N. Lin, and H.S. Chiou: *AFS Trans.*, 1995, vol. 103, pp. 265–73.

18. B.C. Liu, T.X. Li, Z.J. Rue, X.Y. Yang, E.Q. Huo, and C.R. Loper: *AFS Trans*., 1990, vol. 98, pp. 753–57.
19. E. Campomanes: *Giesserei*, 1978, vol. 65, pp. 535–40.
20. T.C. Xi, J. Fargues, M. Hecht, and J.C. Margerie: *Mater. Res. Soc. Symp. Proc*., 1985, vol. 34, pp. 67–76.
21. I. Asenjo, P. Larrañaga, J. Sertucha, R. Suárez, I. Ferrer, J.M. Gómez, and J. Lacaze: *Int. J. Cast Met. Res*., 2007, vol. 20, pp. 319–24.
22. M. Castro, M. Herrera, M.M. Cisneros, G. Lesoult, and J. Lacaze: *Int. J. Cast Met. Res*., 1999, vol. 11, pp. 369–74.
23. M.D. Chaudhari, R.W. Heine, and C.R. Loper: *AFS Trans*., 1974, vol. 82, pp. 379–86.
24. J. Zhou, W. Schmitz, and S. Engler: *Giessereiforschung*, 1987, vol. 39, pp. 55–70.
25. S.-E. Wetterfall, H. Fredriksson, and M. Hillert: *JISI*, 1972, May, pp. 323–33.
26. O. Tsumura, Y. Ichinomiya, H. Narita, T. Miyamoto, and T. Takenouchi: *IMONO*, 1995, vol. 67, pp. 540–45.
27. E.N. Pan and C.Y. Chen: *AFS Trans*., 1996, vol. 104, pp. 845–58.